JOURNAL OF MATERIALS SCIENCE 24 (1989) 3403–3410

Effect of impurities on the weldability of powder metallurgy, electron-beam melted and arc-melted molybdenum and its alloys

FUMIO MORITO
National Research Institute for Metals, 1-2-1 Sengen, Tsukuba 305, Japan

Welds of various molybdenum metals and alloys were examined by bend tests between 183 and 333 K, and the fracture surfaces were observed by scanning electron microscopy and Auger electron spectroscopy. In PM-Mo, blow holes were formed but weldability was improved by selecting high-purity powder, which contained low concentrations in oxides forming impurities, to reduce the total content of oxygen. Nitrogen segregated to grain boundaries promoted intergranular brittleness in PM-Mo. However, in EB-Mo, AM-Mo, Mo–0.56 % Nb and TZM, nitrogen was hardly detected and carbon segregation was always present at grain boundaries. Carbon segregation and carbide precipitation were found to strengthen the grain-boundary cohesion and improve the ductility.

1. Introduction

It has been reported that the presence of impurities such as oxygen, carbon and nitrogen could have a strong effect on the mechanical properties of molybdenum and its alloys [1–4]. These impurities would segregate and precipitate at grain boundaries to enhance intergranular embrittlement. Until recent years, the effect of impurities was analysed by the function of total concentration in the bulk material, but recent progress in microanalyses has enabled understanding of the microstructure and impurity distribution at grain boundaries. In highly purified bicrystals [5], interglanular fracture surfaces were free from foreign elements to the level of sensitivity in the Auger electron spectroscope (AES). Such an intrinsic intergranular brittleness was also observed in an ultra-purified polycrystalline molybdenum [6]. With an AES analysis in a bamboo-type bicrystal of high-purity molybdenum [7], controlled oxygen addition and carbon doping revealed that oxygen segregated to grain boundaries caused intergranular brittleness, but carbon suppressed oxygen segregation at grain boundaries resulting in improved ductility. The direct effect of carbon segregation at grain boundaries has demonstrated that the ductility in coarse-grained molybdenum melted by an electron-beam process was remarkably improved by ageing at about 800 K [8]. Similar ageing around 1000 K has been shown by AES analysis to induce carbon segregation at grain boundaries in a recrystallized molybdenum [9].

Carbide precipitation was also proposed to improve the cohesion of grain boundaries forming low-energy semicoherent interfaces [10, 11]. Welds of a molybdenum alloy, TZM, were studied by AES and revealed that oxygen or other interstitial elements were eliminated as sources of grain-boundary embrittlement [12]. But in the electron beam welded PM-Mo [13], nitrogen segregation was recognized at the grain boundaries in weld metal and was considered to enhance embrittlement of the welds. Postweld heat treatment contributed to the recovery of ductility. Carbon segregation and precipitation by heat treatment strengthened the cohesion of grain boundaries and resulted in improving the ductility [14]. In this study, a variety of electron-beam welds in molybdenum metals and its alloys were tested by bend tests. Microstructure and fracture surfaces were examined to discuss the effect of impurity on the weldability and intergranular embrittlement.

2. Experimental details

Materials used in this study are, as given in Table I, a variety of powder metallurgy molybdenum (PM-1, PM-2 and PM-3), arc-melted molybdenum (AM-1 and AM-2) and TZM, electron-beam melted molybdenum (EB-1 and EB-2) and Mo–0.56 % Nb. Electron-beam welding was carried out under typical conditions such as beam voltage 50 kV, beam current 50 mA, welding speed 30 mm sec^{-1} and vacuum less than 2.7×10^{-2} Pa as shown in Table II. Bend specimens, 1 mm × 3 mm × 25 mm, were tested at a cross-head speed of 1 mm min^{-1}. Heat treatments between 1173 and 1773 K were carried out for 1 h in a vacuum below 2.7×10^{-4} Pa. Carburized annealing was carried out at 1773 K for 30 min after carbon deposition [15]. Fracture surfaces and microstructure were then examined by scanning electron microscopy (SEM) and AES.

3. Results and discussion

3.1. Metallography

Fig. 1 shows the bead pattern surface PM-3 which could not gain sound welds. There appeared sputtered melts, wavy bead edges and disordered bead ripples,

0022–2461/89 $03.00 + .12

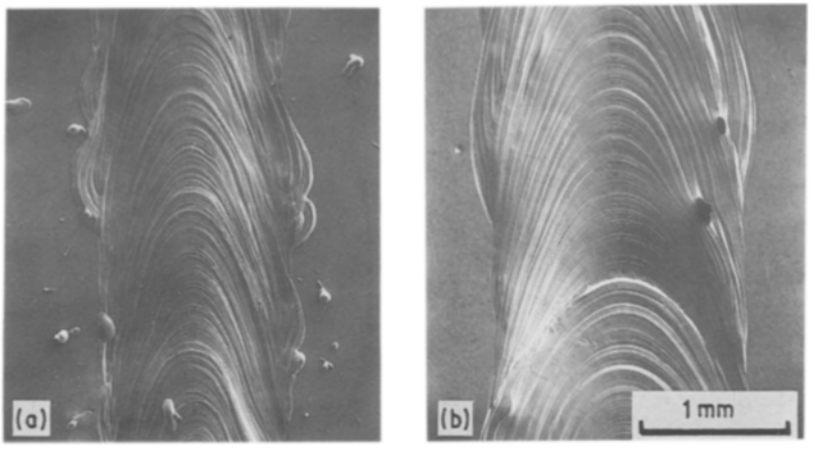

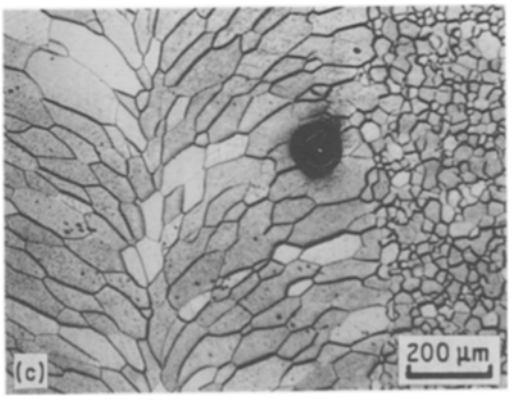

Figure 1 Examples of the bead pattern surfaces in as-welded PM-3. (a) sputtered melts, (b) and (c) blow hole.

as seen in Fig. 1a, in contrast with smooth and straight beads in the sound welds. Large blow holes were sometimes observed even in the bead surface as in Fig. 1b. Blow holes were often found in the bond region near the heat-affected zone as in Fig. 1c.

Fig. 2 shows the sound weld macrostructure of a cross-section of as-welded PM-2, where directionally solidified weld metal with large grains, a heat-affected zone with comparatively small grains, and base metal with rolling texture, were clearly distinguished. PM-1, PM-2 and all other melted materials formed sound welds.

3.2. Bend properties

Fig. 3 shows bend ductility as a function of test temperature in PM-1. The unwelded specimen, which was as-rolled or annealed at 1173 K for 1 h, had superior ductility. They were fully bent even at 183 K. But even sound welds exhibited comparatively low ductility. As-welded and postweld annealed samples showed less ductility than recrystallized base metals at 263 K. Carburized annealing was remarkably effective in improving ductility in both weld and base metal [8, 9, 13–15]. The ductile brittle transition temperature (DBTT) was defined at the bend angle of 5° in this study. The DBTTs in various types of molybdenum and its alloys are listed in Table III. As-welded specimens in PM-1 showed DBTT between 220 and 250 K irrespective of annealing temperature before annealing. Postweld annealing below 1473 K maintained the DBTT at 223 K in the specimen annealed at 1473 K before welding. However, postweld annealing at 1673 K was not effective so that the DBTT increased to 265 K irrespective of preweld annealing. Carburized annealing for PM-Mo remarkably decreased the DBTT to less than 185 K in both weld and base metal. In PM-2, the as-welded specimen revealed a significantly lower DBTT of about 200 K. Postweld annealing at 1173 K increased the DBTT to 216 K. Specimens postweld annealed above 1473 K increased the DBTT to more than 230 K, which was the DBTT in the base metal recrystallized at 1673 K. The DBTTs of the base metal in PM-2 similarly varied with annealing temperature as those in PM-1. Blow holes occurred in the welds of PM-3 as mentioned previously. So the highest DBTT of the as-welded specimen was recognized to be 325 K and that of the postweld annealed one decreased to 271 K showing a considerable improvement in ductility. The DBTT of postweld annealed EB-1 was less than 183 K, which was an almost similar ductility to the recrystallized base metal in EB-1 or postweld annealed EB-2. In EB-2, carburized annealing before welding was more effective than postweld carburized annealing. The DBTT of postweld annealed Mo–0.56 % Nb was very similar to that of the recrystallized

TABLE I Chemical compositions of the materials in this study (wt p.p.m.)

	Al	Mg	Ca	Cu	Si	Mn	W	Ni	Fe	Ti	Zr	Nb	Ta	Cr	C	N	O
PM-1	2.1	1.6	11	3.6	15	< 50		< 50	< 100					< 40	7	6	16
PM-2	< 3	< 0.8	< 2	< 3	15	< 3		5	20						5	6	18
PM-3	< 3	9	5	5											7	6	27
EB-1					66	0.9	280	0.6	2.4		1.6	39	22	2.1	17	3	16
EB-2					90	0.4	57	31	11		25	21	22	8	11	2	21
AM-1															1890		
AM-2															7		
Mo–0.56 % Nb								2	3			5600		5	57	2	10
TZM					10		< 10	20		4500	940				119	6	14

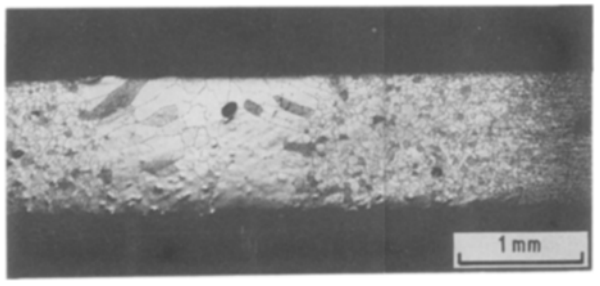

Figure 2 Macrostructure of as-welded PM-2.

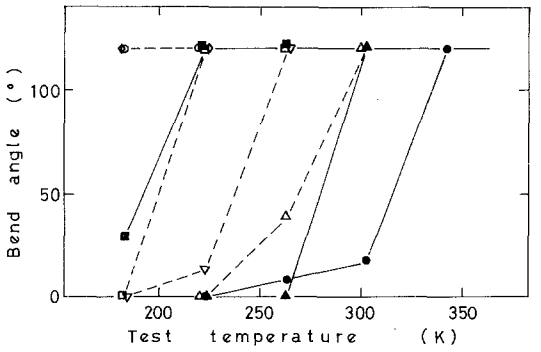

Figure 3 Bend ductility of base metal and weld in PM-1. Base metal: (○) as-rolled, (◇) annealed at 1173 K, (▽) annealed at 1473 K, (△) annealed at 1673 K, (□) carburized at 1773 K. Weld: (●) as-welded, (▲) postweld annealed at 1673 K, (■) postweld carburized at 1773 K.

base metal. As-welded AM-2 revealed low ductility and a DBTT above 343 K, which was considerably higher than that of as-welded AM-1. Welds of TZM showed a slightly higher DBTT between 180 and 200 K than the recrystallized base metal. Postweld carburized annealing for TZM and EB-2 was not as effective in base metal or the weld. EB-Mo and Mo alloys, such as Mo–0.56 % Nb and TZM, were found to have superior bend ductility to PM-Mo and AM-Mo in this experiment.

3.3. Fractography

Welded molybdenum and alloys generally fractured in the weld metal. Cracks initiated at grain boundaries and propagated mainly along the grain boundaries. Below DBTT, premature fracture was often observed, so that welds fractured before yielding at a very low stress. Examples of brittle fracture surfaces are shown in Fig. 4. As-welded AM-1 containing 1890 wt p.p.m. carbon revealed large carbide particles as seen in Fig. 4a. Postweld annealed TZM showed many small precipitates at grain boundaries (Fig. 4b). Carbide precipitates were generally present at grain boundaries in all melted materials except AM-2. It was generally difficult to find an indication of precipitation in PM-Mo. However, postweld carburized PM-1 formed very fine precipitates at grain boundaries as shown in Fig. 4c. Heat-treated welds in PM-Mo exhibited an indication of precipitation in some parts of the intergranular fracture surfaces.

As mentioned previously, carburized annealing greatly strengthened the base material and welds in PM-Mo due to carbon precipitation and improved the ductility except in the case of TZM and EB-2 weld. Microporosities were observed in the cleavage fracture surfaces as well as in the grain-boundary fracture surfaces in almost all cases. However, their influence on mechanical properties seemed to be not so significant, because sphere-like defects with a very small size and diffuse density were insensitive to notch effect [13, 14, 19].

Fig. 5 shows the fracture surface and AES map which contained blow holes in the weld metal of PM-3. No other peaks except those of molybdenum were observed in the smooth grain boundaries. Oxygen, potassium and calcium were enriched within the blow holes suggesting that oxides were formed and vapourized during welding.

TABLE II Electron-beam welding conditions

Accelerating voltage	50 kV
Beam current	50 mA
Welding speed	30 mm sec^{-1}
Work distance	175 mm
Focus	surface
Joint type	bead on plate
Vacuum	$< 6.7 \times 10^{-2}$ Pa

3.4. Effect of nitrogen

Auger electron spectra taken from fracture surfaces are shown in Fig. 6. Intergranular fracture surfaces in as-welded PM-1 clearly indicated nitrogen segregation, as seen in Fig. 6a. After postweld annealing at 1673 K, there was no detectable impurity peak (Fig. 6b) which resembled the case of unwelded recrystallized PM-1. The total nitrogen content in the weld metal was not significantly changed after electron-beam welding and there was no indication of such a profuse nitrogen segregation in the case of melted molybdenum and alloys. Therefore, nitrogen segregation occurred mainly from redistribution of nitrogen in the bulk and partly from the welding atmosphere during welding and cooling. A sputter experiment indicated that nitrogen segregation was limited to the near surfaces of intergranular fracture. However, it was difficult to distinguish the chemical state of nitrogen segregation at the grain boundaries in this experiment. Following the standard quantitative method [16], nitrogen concentration at grain-boundary regions was compared to the yield stress at DBTT as shown in Fig. 7. According to the detailed work on brittle behaviour of molybdenum at low temperature [17], the yield stress at DBTT was considered to be critical yield stress (σ_c) which was nearly equal to crack propagation stress or crack nucleation stress. In as-welded PM-Mo which contained about 20 at % nitrogen at grain boundaries, an increase in nitrogen at grain boundaries tended to decrease the critical yield stress and increase the DBTT. This reflected not only the effect of nitrogen concentration at grain boundaries but also microstructure in the weld. For example, blow holes in as-welded PM-3 seemed to promote weakening of the critical yield stress and an increase in DBTT. However, after postweld annealing at 1673 K, nitrogen disappeared and the DBTT and the critical yield stress became about 250 K and about 500 MPa, respectively. Thus nitrogen segregation was qualitatively detrimental to grain-boundary cohesion in

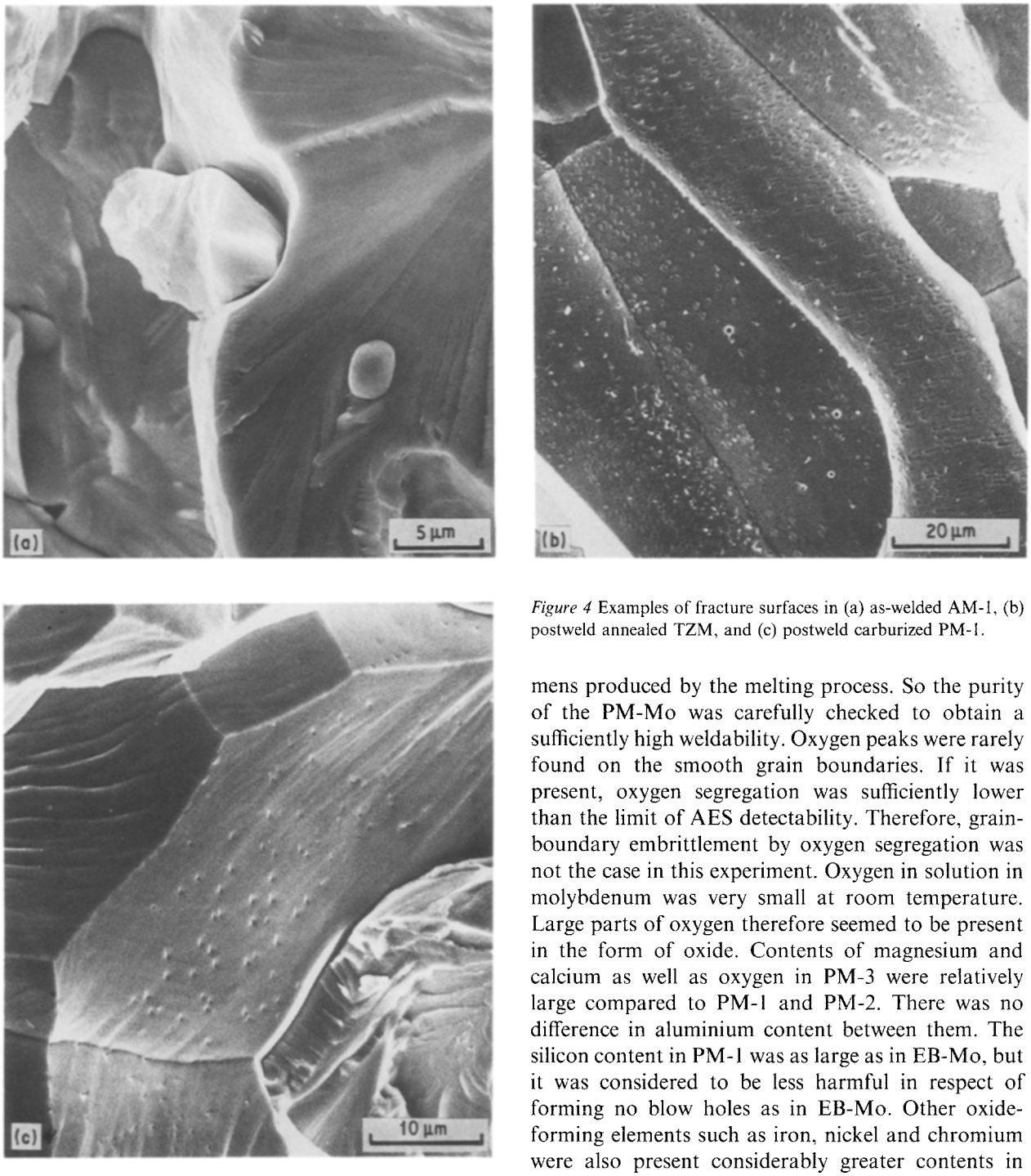

Figure 4 Examples of fracture surfaces in (a) as-welded AM-1, (b) postweld annealed TZM, and (c) postweld carburized PM-1.

as-welded PM-Mo. Nitrogen was suggested to promote low interatomic bonding in the grain-boundary structures. Nitrogen–nitrogen bonding or nitrogen–molybdenum bonding seemed to decrease grain-boundary cohesion. Further study is required to understand the detailed nitrogen structure at grain boundaries.

3.5. Effect of oxygen

When an AES spectrum was taken from the microporosity or the oxide particles on grain boundaries in as-welded PM-1, aluminium, phosphorus, sulphur, potassium and calcium, as well as oxygen, were often observed. As mentioned before, potassium and calcium with oxygen were enriched in the blow holes of PM-3. However, it was difficult to observe such particles and no blow holes were found in other specimens produced by the melting process. So the purity of the PM-Mo was carefully checked to obtain a sufficiently high weldability. Oxygen peaks were rarely found on the smooth grain boundaries. If it was present, oxygen segregation was sufficiently lower than the limit of AES detectability. Therefore, grain-boundary embrittlement by oxygen segregation was not the case in this experiment. Oxygen in solution in molybdenum was very small at room temperature. Large parts of oxygen therefore seemed to be present in the form of oxide. Contents of magnesium and calcium as well as oxygen in PM-3 were relatively large compared to PM-1 and PM-2. There was no difference in aluminium content between them. The silicon content in PM-1 was as large as in EB-Mo, but it was considered to be less harmful in respect of forming no blow holes as in EB-Mo. Other oxide-forming elements such as iron, nickel and chromium were also present considerably greater contents in PM-3. So it was desirable to decrease these elements in order to reduce the oxygen content as much as possible in the material. At the same time, it was also desirable to reduce elements such as phosphorus, sulphur and potassium, which were not analysed as in Table I. When the total content of oxygen was lowered to less than 20 wt p.p.m. as in melted materials, by selecting higher purity powder and severe process control during sintering and following heating and rolling, sound welds could be obtained reproducibly in PM-Mo.

3.6. Effect of carbon

Fig. 8 shows the critical yield stress and the DBTT as a function of carbon concentration at grain boundaries in PM-Mo. With an increase in carbon at grain boundaries, the critical yield stress increased from 900 to 1250 MPa in base metal and from 550 to above

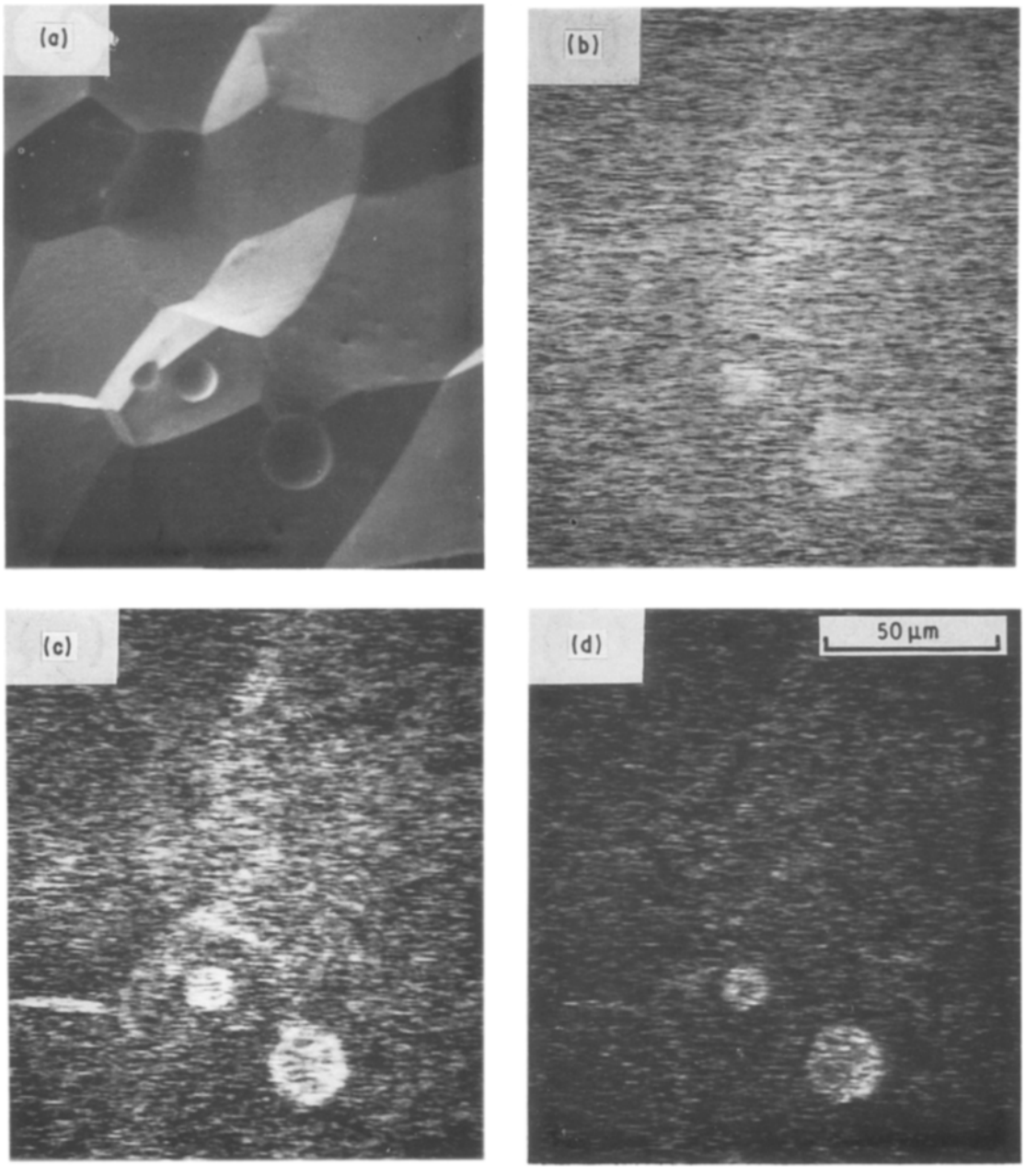

Figure 5 AES maps of as-welded PM-3: (a) secondary electron micrograph, (b) calcium image, (c) oxygen image and (d) potassium image.

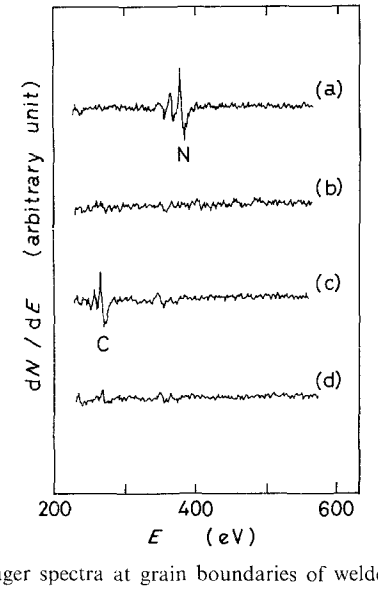

Figure 6 Auger spectra at grain boundaries of welded PM-1: (a) as-welded, (b) postweld annealed, (c) postweld carburized, and (d) as-welded specimen with annealing at 1673 K before welding.

1000 MPa in the weld. The DBTT of base metal correspondingly decreased from 230 to 185 K and that of the weld from 270 to less than 183 K. It was not difficult to find precipitates in the specimen which contained less than 10 at % carbon at grain boundaries. This fact means that carbon segregation contributed to the enhancement of cohesion of grain boundaries and improved ductility. As shown in Fig. 6c, there is clearly a rise in carbon peak of more than 20 at % on the fracture surface of postweld carburized PM-1. This carburization increased the total carbon content to about 27 wt p.p.m., so that a net increase of 20 wt p.p.m. carbon contributed to precipitate fine carbides as seen in Fig. 4c and the ratio of cleavage fracture surfaces also increased. Therefore it was demonstrated that carbon precipitation as well as carbon segregation was effective in strengthening the grain-boundary cohesion [20].

Fig. 9 shows that the carbon segregation at smooth grain boundaries in melted specimens varied between

13% and 30%. These specimens generally showed carbide precipitates at grain boundaries, as mentioned previously. The critical yield stress was above 1400 MPa in as-welded or carburized EB-2 before welding. It decreased to 850 MPa after postweld heat treatment, which was nearly the same as that of recrystallized base metal or postweld annealed EB-1. That of TZM, both in base metals and welds, was above 1400 MPa, irrespective of heat treatment. That of postweld annealed Mo–0.56 % Nb showed a higher value of about 1050 MPa. The DBTTs of these specimens were all less than 195 K. Accordingly, carbon segregation and precipitation were demonstrated to improve ductility due to an increase in grain-boundary cohesion in melted molybdenum metals and alloys. Recently, it was reported that the effect of carbon impurity on grain-boundary fracture is structure dependent in the ⟨1 1 0⟩ Mo bicrystals [18]; Carbon dissolved or precipitated at a grain boundary increases the cohesion of the intrinsically weak boundaries and decreases the cohesion of the intrinsically strong boundaries. But, as for polycrystalline specimens in this study, carbon segregation and precipitation were generally very effective in improving ductility in welds and base metals. A large number of excess carbons, however, formed large precipitate particles at grain boundaries and within grain interiors, resulting in a hardening of the grain boundary zone and precipitate–matrix interfaces. Thus it decreased cohesion of grain boundaries and interfaces and fractured in a brittle manner as in the weld of AM-1. Depth profiles were obtained by argon-ion bombardment, but it was difficult to distinguish the state of carbon in this sputter experiment by adsorption of carbon and oxygen from the atmosphere. Further study to understand structure and chemical state of carbon bonding must also be performed.

4. Conclusions

Bend properties of electron-beam welds in various types of molybdenum and its alloys were examined and microstructure and fracture surfaces were evaluated. The main impurity effects on the weldability are summarized as follows.

1. Blow holes were formed in PM-Mo with oxygen higher contents which contained considerable

TABLE III Ductile–brittle transition temperature of base metal and weld in molybdenum and its alloys

Alloy	Condition		DBTT (K)
PM-1	Base metal	As-rolled	< 183
		Annealed at 1173 K	< 183
		1473 K	199
		1673 K	229
		Carburized	185
	Weld	As-welded	249
		Postweld annealed at 1673 K	265
		Carburized	< 183
		Annealed at before welding 1473 K	
		As-welded	223
		Postweld annealed at 1173 K	223
		1473 K	223
		Annealed at before welding 1673 K	
		As-welded	233
		Postweld annealed at 1673 K	265
		Carburized	< 183
PM-2	Base metal	As-rolled	< 183
		Annealed at 1173 K	< 183
		1473 K	189
		1673 K	231
	Weld	As-welded	203
		Postweld annealed at 1173 K	216
		1473 K	264
		1673 K	239
PM-3	Weld	As-welded	325
		Postweld annealed at 1673 K	271
EB-1	Base metal	Annealed at 1673 K	187
	Weld	Postweld annealed at 1673 K	183
EB-2	Weld	As-welded	< 183
		Postweld annealed at 1673 K	< 183
		Carburized	187
		As-welded with carburization before welding	< 183
AM-1	Weld	As-welded	270
AM-2	Weld	As-welded	> 343
Mo–0.56 % Nb	Base metal	Annealed at 1673 K	189
	Weld	Postweld annealed at 1673	191
TZM	Base metal	As-rolled	< 183
		Annealed at 1773 K	< 183
		Carburized	< 183
	Weld	As-welded	187
		Postweld annealed at 1773 K	183
		Carburized	195

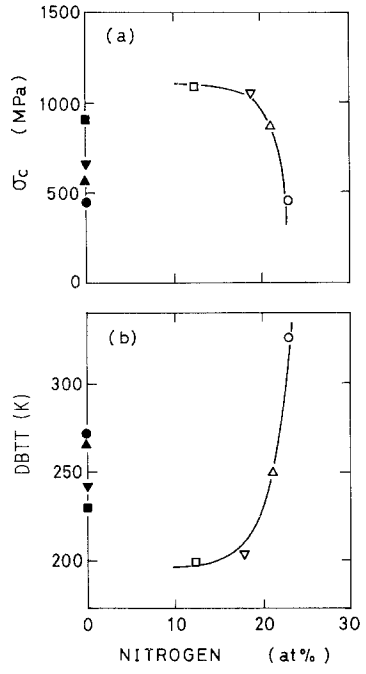

Figure 7 (a) Critical yield stress and (b) DBTT as a function of nitrogen content at grain boundaries in PM-Mo. (□) Base metal of PM-1 recrystallized at 1473 K, (■) base metal of PM-1 recrystallized at 1673 K, (△) as-welded PM-1, (▲) PM-1 postweld annealed at 1673 K, (▽) as-welded PM-2, (▼) PM-2 postweld annealed at 1673 K, (○) as-welded PM-3, (●) PM-3 postweld annealed at 1673 K.

quantities of oxide-former impurities. AES exhibited that no oxygen was observed at smooth grain boundaries, but blow holes and oxide particles often contained aluminium, phosphorus, sulphur, potassium and calcium. Other oxide-forming metallic impurities, such as silicon, magnesium, iron, nickel and chromium are desired to be reduced as much as possible. Sound welds were obtained when the total oxygen was lowered to less than 20 wt p.p.m.

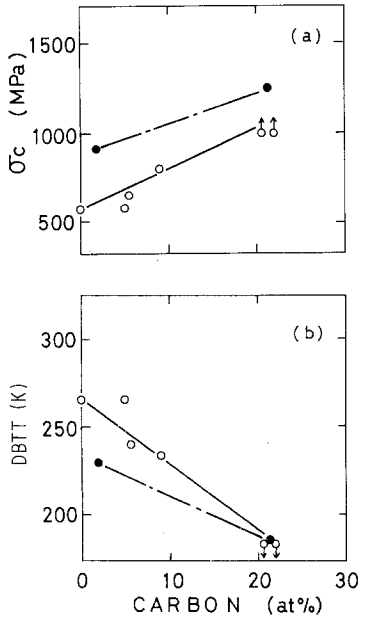

Figure 8 (a) Critical yield stress and (b) DBTT as a function of carbon content at grain boundaries in PM-Mo. (●) Base metal, (○) weld.

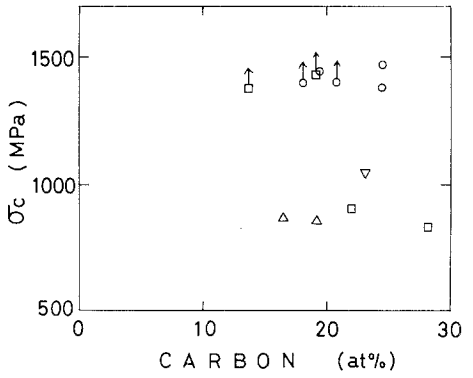

Figure 9 Critical yield stress as a function of carbon content at grain boundaries in melted molybdenum and its alloys. (△) EB-1, (□) EB-2, (○) TZM, (▽) Mo–0.56 % Nb.

2. Nitrogen segregation was observed in as-welded PM-Mo and promoted decohesion of the grain boundary resulting in a decrease of ductility.

3. Melted molybdenum and its alloys generally eliminated oxygen and nitrogen segregation at grain-boundary surfaces in weld metal. Therefore, their bend properties tended to be superior to those of PM-Mo. It was indicated that weldability was generally affected by the characteristics of the base metal itself.

4. Heat-treated or carburized PM-Mo and melted molybdenum and its alloys showed that carbon segregation and precipitation enhanced cohesion of the grain boundary and improved the ductility.

Acknowledgements

The author thanks Drs H. Irie and S. Tsukamoto for performing the electron beam welding experiments and for fruitful discussions. Dr T. Noda is thanked for his invaluable comments on the manuscript, as are the many colleagues in Tsukuba Laboratories for their useful support and assistance during the period of this work.

References

1. L. E. OLDS and G. W. P. RENGSTORFF, *J. Metals* **8** (1956) 150.
2. T. TAKAAI, *J. Jpn Inst. Metals* **28** (1964) 676.
3. G. K. ZELENSKIY, V. D. BORODICH, S. I. SIRYUKOV and V. K. KORONTSEVICH, *Fiz. Metal Metalloved.* **35** (1973) 622.
4. J. P. TOUBOUL, L. MINEL and J. P. LANGERON, *J. Less-Common Metals* **30** (1973) 279.
5. J. B. BROSSE, R. FILLIT and M. BISCONDI, *Scripta Metall.* **15** (1981) 619.
6. G. LORANG, P. AILLOUD, L. DEBOVE, J. C. ROUCHAUD, M. FEDOROFF and J. P. LANGERON, *Z. Metallkde* **74** (1983) 458.
7. A. KUMAR and B. L. EYRE, *Proc. Roy. Soc. London* **A370** (1980) 431.
8. K. TSUYA and N. ARITOMI, *J. Less-Common Metals* **15** (1968) 245.
9. S. SUZUKI, H. MATSUI and H. KIMURA, *Mater. Sci. Engng* **47** (1981) 209.
10. A. KUMAR and B. L. EYRE, *Acta Metall.* **26** (1978) 569.
11. R. KISHORE and A. KUMAR, *J. Nucl. Mater.* **101** (1981) 16.
12. J. WADSWORTH, G. R. MORSE and P. M. CHEWEY, *Mater. Sci. Engng* **59** (1983) 257.
13. F. MORITO, *J. Less-Common Metals* **146** (1989) 337.
14. F. MORITO, *J. Nucl. Mater.* (1989) in press.

15. Y. HIRAOKA, F. MORITO, M. OKADA and R. WATANABE, *J. Nucl. Mater.* **78** (1978) 192.
16. L. E. DAVIS, N. C. MacDONALD, P. W. PALMBERG, G. E. RIACH and R. E. WEBER, "Handbook of Auger Electron Spectroscopy", 2nd Edn (Physical Electronics Industries, Inc., Eden Prairie, Minnesota, 1976).
17. A. S. WRONSKI, A. C. CHILTON and E. M. CAPRON, *Acta Metall.* **17** (1969) 751.
18. H. KURISHITA, A. OISHI, H. KUBO and H. YOSHINAGA, *J. Jpn Inst. Metals* **47** (1983) 546.
19. E. MORITO, Proceedings 12th International Plansee Seminar, edited by H. Bildstein and H. M. Ortner, Vol. 1 (1989) p. 417.
20. *Idem, ibid.*, Vol. 1 (1989) p. 313.

Received 1 September 1988
and accepted 2 January 1989